Nuclear Engineering and Design 417 (2024) 112868

Contents lists available at ScienceDirect

Nuclear Engineering and Design

journal homepage: www.elsevier.com/locate/nucengdes

Neutronic evaluation for different external neutron sources in a Small-Subcritical fast reactor

Renato Vinícius A. Marques, Carlos E. Velasquez, Claubia Pereira *

Departamento de Engenharia Nuclear, Escola de Engenharia – UFMG, Av. Antônio Carlos, 6627 - Pampulha, Belo Horizonte MG, Brazil

ARTICLE INFO

Keywords:
Small subcritical fast reactor
Fusion source
Evaporation source
Transmutation
Actinide
Transuranic
Neutronic parameters
Fuel burnup
Thorium

ABSTRACT

This study proposes an optimized small-sized subcritical fast reactor with an external neutron source for actinide transmutation. The reactor integrates features of Accelerator Driven Systems (ADS) and Fusion-Fission Systems (FFS) based on Tokamak technology. Both external neutron sources were evaluated, one from fusion reactions and the other from spallation reactions in the designed small subcritical fast reactor. The analysis assessed neutron flux and actinide transmutation rates through fuel burnup simulations at 1200 K. The results underscore the significance of external neutron sources in subcritical systems, with the fusion-fission source presenting high actinide transmutation. The SSFR utilizes thorium oxide as fuel and Lead-Bismuth Eutectic (LBE) as coolant. Neutronic parameter comparisons between FFS and ADS neutron sources were conducted, showing advantages for actinide transmutation in the system with the FFS neutron source, which enhances transmutation, minimizing radiotoxicity. The neutronic parameters were obtained using the MCNP, while the MONTEBURNS code, which links the MCNP and the ORIGEN depletion code, was utilized to perform the fuel burnup simulations. The cross-section libraries were generated by the NJOY-2012 using the nuclear data library JEFF-3.3.

1. Introduction

Currently, nuclear power plants produce more than one-quarter of all low-carbon electricity in the world, which avoided the emission of about 70 gigatonnes (Gt) of carbon dioxide (CO_2) - equivalent to the emissions from the entire global power sector in the five years nuclear energy (IAEA, 2022). However, radioactive waste management represents a great challenge nowadays due to the long-lived and high radiotoxicity waste present in the spent fuels from conventional nuclear power plants. The better way to decrease the radiotoxicity of the transuranic of the spent fuel is inducing fission, and hybrid systems such as Accelerator-Driven System (ADS) and Fusion-Fission Systems have been studied as a way to achieve this end. These systems offer enhanced safety in reactor operation control and shutdown in subcritical mode, mainly decreasing the long-lived radiotoxicity waste (Gilberti et al., 2015).

There are many proposals for ADS and FFS for different purposes. Concerning the Accelerator-Driven Systems, Esam M.A. Hussein concluded that the ADS can potentially improve the neutron economy, which is related to the neutron abundance of the spallation process (Esam, 2020). The Japan Atomic Energy Research Institute (JAERI) researched the development of a superconducting proton linear accelerator and the radiation damage in materials (Saito, 2006). Additionally, T. Minh (2021) investigated using liquid metal LBE as a spallation target and coolant for the ADS system, achieving high neutron production and flux in the ADS with molten LBE. According to De-Peng Guo et al. (2016) and P. Zhivkov et al. (2018), the ADS has been universally considered the most efficient for disposing of highly radioactive waste. However, the central focus of these studies was investigating the cooling system's influence on neutron flux and energy production in the ADS. Further, Deng et al. (2021) investigated the space–time kinetics of the ADS during neutron beam transients to ensure the reliability of the subcritical system's control and safety, emphasized the influence of the external neutron source and subcriticality on kinetic parameters, especially neutron generation time (NEA, 2002). However, unlike the fusion-fission systems, ADS is more significant for breeding than transmutation applications (Esam, 2020).

Regarding the fusion-fission hybrid systems (FFS), Plukienė et al. (2018) analyzed the performance of a fusion-fission hybrid system by comparing actinide transmutation scenarios using spent nuclear fuel from reactors in Sweden (LWR) and Lithuania (RBMK). According to Bedenko et al. (2022), the concept of a hybrid reactor with a deuterium–tritium (D-T) linear neutron plasma source allows the operation in

* Corresponding author.
E-mail address: claubia@nuclear.ufmg.br (C. Pereira).

https://doi.org/10.1016/j.nucengdes.2023.112868
Received 21 October 2023; Received in revised form 18 December 2023; Accepted 19 December 2023
Available online 27 December 2023

a subcritical mode, significantly enhancing nuclear safety levels. Hong and Kim (2018) investigated the feasibility of directly reusing spent nuclear fuel in a hybrid fusion-fission system, conducting analyses on the effective transmutation of transuranic nuclides into transuranic fuels diluted with uranium and zirconium, the required fusion power, and the tritium production ratio. Moreover, Şahin et al. (2018) concluded that mixing spent light water reactor fuel with thorium can result in higher burnup values than conventional light water reactors.

Regarding the subcritical system studies, Lafuente and Piera (2011) showed the sustainability and potential of nuclear materials exploitation by the burnup achieved in subcritical nuclear reactors. Zafar and Kim (2018) analyzed the effects of an external neutron source in a subcritical reactor approaching the external source with an embedded fission source. In addition, Lei Ren et al. (2021) studied the Mo-99 production in a subcritical system driven by an external fusion source using low-enriched uranium. Moreover, Barros et al. (2021) investigated and compared the capabilities of a spallation source and a fusion source in a subcritical system that was loaded with a hexagonal lattice formed by 120 thorium rods and 36 rods of reprocessed fuel mainly for thorium regeneration.

Although the studies on subcritical systems such as ADS and Fusion-Fission are being widely developed worldwide, the advantage of the two systems combined for the actinide transmutation purpose has not been analyzed. Above all, the Nuclear Engineering Department at Universidade Federal de Minas Gerais (DEN/UFMG) has been studying hybrid nuclear reactors for the transmutation of transuranic isotopes, such as Accelerator Driven System and Fusion-Fission System (Velasquez et al., 2016; Marques et al., 2020). Nevertheless, a study of an optimized small-sized subcritical system designed with specific fusion and ADS external neutron sources for neutronic analysis, such as a fuel burnup simulation, has not been done. Furthermore, previous works in FFS showed that the high-energy neutrons from fusion reactions increase the probability of inducing transmutation in transuranic nuclides by fission reactions due to a high probability of fission per absorbed neutron for all the actinides in a hardened neutron spectrum (Velasquez et al., 2016; Marques et al., 2020). Therefore, an optimized small-sized subcritical system modeled at 379 MWt with an external neutron source at the reactor's center was designed to achieve high transmutation of actinides. The goal is to evaluate the transmutation parameters of this designed small-sized nuclear reactor by comparing two different external neutron sources coupled in the center of the nuclear core in the modeled system: the system with a deuterium–tritium (D-T) fusion external source (Marques et al., 2020) comparing to the system with an ADS external source.

The proposed subcritical fast reactor used the fuel from the spent fuel reprocessed by the GANEX (Group ActiNide Extraction) technique (Aneheim, 2012; Miguirditchian et al., 2008) than spiked with thorium (Th) as a nuclear fuel. The GANEX reprocessing technique is composed of two extraction cycles following the dissolution of the spent fuel in nitric acid. Uranium (U) is selectively extracted before the group separation of transuranic elements (Neptune, Plutonium, Americium, Curium), which occurs in the second cycle (Aneheim, 2012; Miguirditchian et al., 2008). The choice of thorium (3 to 4 times more abundant than uranium, widely distributed in nature as an easily exploitable resource in many countries) was based on its fuel cycle, which is an attractive way to produce long-term nuclear energy with low radiotoxicity waste, which has less transuranic elements than uranium (Şahin et al., 2018; IAEA, 2005). In other words, the SSFR uses actinide nuclides as fuel material to transmute them and reduce their radiotoxicity levels. The Lead-Bismuth Eutectic (LBE) was used as the coolant material, and thorium oxide was used as the breeder material in the breeder core (Marques et al., 2020).

The SSFR assessment compared the neutronic parameters, such as criticality, capture-to-fission ratio, neutron spectrum of the external sources, and neutron flux over the core of a semi-heterogeneous SSFR, using the fusion external neutron source (Marques et al., 2020) and an evaporation external source (Rubbia et al., 1995), defined at the same volume in the center of the SSFR. The analyses considered the system at the beginning of life and during a fuel burnup simulation.

2. Methodology

In this section, are presented the designed SSFR, as well as the definition of the external neutron sources. Furthermore, the fuel composition and the defined simulation tools for proper analysis are also described in this section.

2.1. The SSFR model

The SSFR proposed in this study was based on previous studies considering the ADS geometry from Rubbia et al. (1995) redesigned as a small subcritical reactor in a semi-heterogeneous way. The SSFR comprises an iron tank cylinder with an external neutron source at the system's center, as shown in Fig. 1. The SSFR parameters, such as power, number of fuel assemblies per region, dimensions, volumes, and materials are presented in Table 1. A semi-heterogeneous hexagonal lattice divided into an inner and outer core filled with reprocessed fuel and a breeder core filled with thorium oxide represents the reactor core.

The designed fuel lattice in the SSFR was modeled consisting in 120 fuel assemblies. First, each fuel assembly contains around 331 to 397 fuel rods, as shown in Fig. 2-a. To decrease the time of the simulations and optimize the system, the fuel rods inside the assembly were homogenized into a single fuel pin for the analyzes, maintaining the coolant-to-fuel volume ratio, as shown in Fig. 2-b.

2.2. Fusion source definition

The D-T fusion neutron spectrum, used as the external neutron source, was obtained by calculating in the MCNP5 the neutron flux over the surface of the first wall from the FFS based on Tokamak, which has already been studied (Marques et al., 2020) for the energy range 10^{-9} to 14.1 MeV. The obtained neutron spectrum was normalized over the total flux. Then, the normalized fusion neutron spectrum was designed as an external source defined in the entire volume (41.53 dm^3) at the center of the SSFR with a radius of 7.5 cm.

2.3. Spallation source definition

The spallation source is essential for the ADS reactor concept (Rubbia et al., 1995). In this system, a high-energy proton accelerator is used to generate a high-intensity beam of protons that is directed onto a Lead (Pb) target, producing neutrons by spallation reactions that are used to drive the subcritical reactor (Rubbia et al., 1995). The ADS spallation source was defined in the modeled SSFR considering the Pb material in

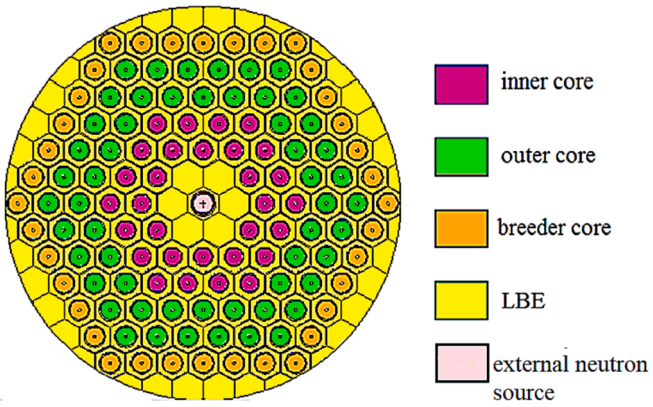

Fig. 1. Overview of semi-heterogeneous SSFR system.

Table 1
Main parameters of the modeled Small Subcritical Fast Reactor.

Geometry and Power		
Power (MWt)		379
Active Height (cm)		102.5
Height (cm)		235
Core Radius (cm)		150
External source radius (cm)		7.5
Clad Thickness (cm)		0.18
Inner Fuel rod radius (cm)		6.64
Outer Fuel rod radius (cm)		7.27
Breeder Fuel rod radius (cm)		7.27
Fuel assembly radius (cm)		11.6
Number of fuel assemblies in the inner core		30
Number of fuel assemblies in the outer core		54
Number of fuel assemblies in the breeder core		36
External source volume (dm^3)		41.53
Total volume (m^3)		41.93
Materials		**Temperature (K)**
Coolant	LBE	613.5
Fuel Rod Inner Gas	He	1200
Clad	HT-9	900
Fuel	Spent fuel reprocessed by the GANEX technique spiked with ThO_2	1200

the entire source volume (41.53 dm^3). The neutron energy distribution was designed in the MCNP code by the Evaporation Source (ES) energy spectrum, described by Rubbia et al. (1995):

$$p(E) = CEexp(-E/a) \quad (1)$$

where $a = 1.2895$ MeV.

To compare the neutron spectrum from each external source in the system, Fig. 3 shows the neutron spectrum from the fusion source and the evaporation source in the SSFR. The evaporation external source presents higher neutron flux, almost in the entire energy range, than the fusion source. However, for the hardened neutron range (above 3 MeV energy), the fusion source presents greater neutron flux than the evaporation source due to the 14.1 MeV neutrons emitted in the D-T fusion reaction, which increases the actinide transmutation by fission reactions.

2.4. Fuel material

The fuel composition was obtained by reprocessing spent nuclear fuel from a standard Pressurized Water Reactor (PWR) fuel with an initial enrichment of 3.1 %, which had undergone a fuel burnup of 33,000 MWd/t and was kept in a spent fuel pool for five years (Cota and Pereira, 1997). The spent nuclear fuel was reprocessed using the GANEX technique (Aneheim, 2012; Miguirditchian et al., 2008). Then, the reprocessed fuel was spiked with thorium oxide and assigned to the inner and outer cores. The weight percentage of fissile material was 11.25 %, as shown in Table 2, to achieve a subcritical condition safer for the SSFR. Thorium oxide was used in the breeder core to produce fissile material.

2.5. Simulation

At the Beginning Of Life (BOL) and full power, the SSFR system was modeled using the Monte Carlo N-Particle Transport Code Version 5 - MCNP5 (X-5 Monte Carlo Team, 2003). The simulation used 10^8

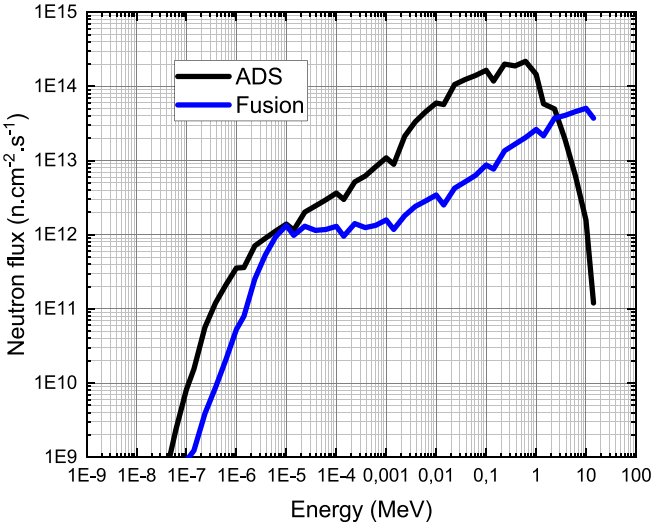

Fig. 3. Neutron spectra of different external sources.

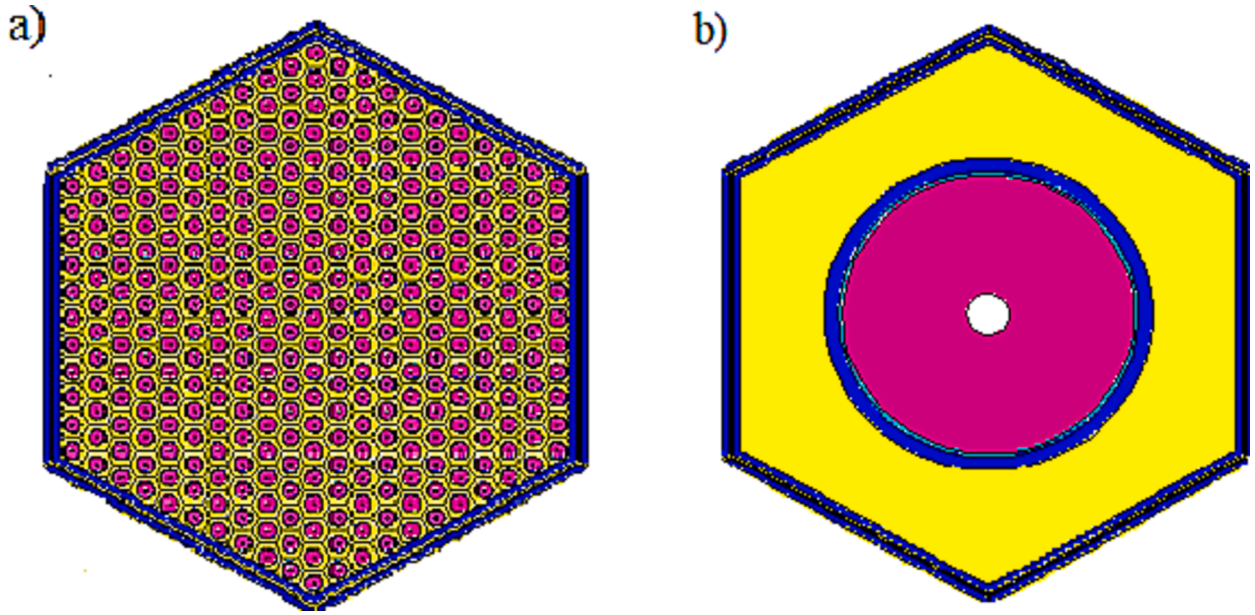

Fig. 2. The SSFR fuel lattice designed: a) Heterogeneously (a); b) Semi- heterogeneously.

Table 2
Fuel composition: GANEX spiked with ThO_2.

Isotope	Nuclear fuel (wt%)	Isotope	Nuclear fuel (wt%)	Isotope	Nuclear fuel (wt%)
Th-232	7.1421E + 01	Np-239	5.9748E-02	Cm-242	3.282E-02
U-233	2.6431E-09	Pu-238	2.8554E-01	Cm-244	3.7625E-02
U-234	2.3969E-04	Pu-239	7.477E + 00	Cm-245	1.3093E-03
U-235	1.2474E-02	Pu-240	2.5561E + 00	Nd-143	1.9076E-01
U-236	6.3767E-03	Pu-241	2.4034E + 00	Sm-150	3.8255E-02
U-237	7.4863E-06	Pu-242	9.0829E-01	Eu-153	8.1344E-03
U-238	1.5164E + 00	Am-241	1.054E-01	O-16	1.2063E + 01
Np-237	7.0093E-01	Am-242^m	1.9397E-04		
Np-238	9.4628E-04	Am-243	1.737E-01		

particles (nps) to minimize the relative error (approximately 10^{-4}). The Jointly Evaluated Fission and Fusion File-Version 3.3 - JEFF3.3 nuclear data (Nuclear Energy Agency, 2017) was processed for the full power conditions through the NJOY Nuclear Data Processing System-Version 2012 (MacFarlane, 2012). The SSFR analyses were carried out at 1200 K fuel temperature (Marques et al., 2020) for both ADS and fusion external sources to evaluate the differences in the neutronic parameters between them. All simulations kept the LBE coolant temperature constant at 613 K (Marques et al., 2020).

The fuel burnup simulations were performed using MONTEBURNS (Poston and Trellue, 1999), which links the MCNP5 to the ORIGEN2.1 depletion code (Croff, 1980). ORIGEN2.1 uses the neutronic parameters obtained from MCNP to perform fuel burnup, which includes the buildup, decay, and processing of radioactive materials. The new isotopic composition obtained from ORIGEN2.1 is then fed back to MCNP5 to calculate the neutronic parameters of the new composition, and so on, until each cycle is completed. At the end of each cycle, the MONTEBURNS performs neutronic calculations, such as energy per fission, flux normalization, reactor physics constants, effective multiplication factor, and isotopic composition (Poston and Trellue, 1999; Croff, 1980).

The major fission products considered due to their great amount after the burnup simulation in the fuel composition were Krypton (Kr), Strontium (Sr), Yttrium (Y), Zirconium (Zr), Molybdenum (Mo), Technetium (Tc), Ruthenium (Ru), Rhodium (Rh), Palladium (Pd), Tellurium (Te), Iodine (I), Xenon (Xe), Cesium (Cs), Barium (Ba), Lanthanum (La), Cerium (Ce), Praseodymium (Pr), Neodymium (Nd), Promethium (Pm), Samarium (Sm), Europium (Eu), and Gadolinium (Gd) (Cota and Pereira, 1997; Ogata et al., 2020).

This study evaluates some aspects of fuel burnup and reactor performance, such as the neutron flux over time, capture-to-fission ratio, effective multiplication factor, power generation by each fuel isotope, actinide and transuranic transmutation in the SSFR for both evaporation and fusion external sources. To increase the accuracy of the burnup calculation, a "predictor" step is used in which ORIGEN2 is running halfway through the designated burn step. One-group cross-sections are then calculated at the midpoint of the burn step by MCNP. This assumes that the isotopics of the system at the midpoint are a reasonable approximation of the isotopics over the entire burn step. So, it was considered the number of particle histories (nps) equal to 10^6 to increase this accuracy, which includes 40 internal cycles with 10 steps per cycle - each step containing 182,5 days, being more accurate due to the long irradiation periods being broken up into smaller lengths of time The average power density in the system was calculated at 200 W/cm^3 per day. In this context, it was defined in the MONTEBURNS a fission power of 110 MWt for a 5 years fuel burnup simulation, with an average recoverable energy per fission defined in 200 MeV in the aforementioned MCNP model. The materials considered in the fuel burnup simulation were those present in the inner, outer, and breeder core, considering the entire volume of each core region.

3. Results

3.1. Begin of life (BOL)

Fig. 4 shows the neutron spectrum from both evaporation and fusion external sources in SSFR. On the one hand, the fusion external source from the D-T fusion reactions emits discrete neutrons of 14.1 MeV. In contrast, the evaporation source has a more continuous spectrum distribution in the fast energy range. As a result, the neutron flux from the evaporation external source (ES) is more significant than that from the fusion external source (FS) for an energy range of 0.3 to 10 MeV, which could increase the actinide transmutation. Furthermore, the neutron flux in the epithermal energy range is lower than that from the fusion source, which decreases neutron absorption in the resonance range of cross-sections. On the other hand, the neutron flux from the fusion external source is the highest across most of the energy spectra (except for the 0.3 to 10 MeV range), mainly between the 10 to 14.1 MeV energy range.

Table 3 presents the effective multiplication factor (k_{eff}) for the analyzed systems at full power. The k_{eff} values for the different external sources were very similar. When considering the fusion source (D-T), the fusion external source showed slightly lower k_{eff} values than the evaporation source due to higher neutron absorption in the source region of the SSFR with the fusion external source (D-T) than in the SSFR with the evaporation external source (Pb). Additionally, the neutron spectrum is higher in the fast energy range than in the fusion source in SSFR, which could enhance the probability of inducing fission reactions in transuranic nuclides. The absolute difference - in percent mille (pcm) between them indicates few neutronic effects in the SSFR for the analyzed external sources in the system.

Table 4 presents the neutronic parameters, such as the average number of neutrons produced per fission (ν), the average fission neutrons produced per neutron absorbed (η), the thermal utilization factor (f), the fast fission factor (ε), the average neutron lethargy (u), the prompt removal lifetime (l), the effective delayed neutron fraction (βeff) and the capture-to-fission ratio (σγ/σf) in the SSFR for the analyzed external sources.

The ν had equal values regardless of the external source in the system due to the same fuel composition in both systems. However, the η was slightly higher in the SSFR with the FFS source than the ADS source, considering all cells with fission, indicating high fission neutron production at the fuel with FFS external source and neutron economy. Nevertheless, the η values considering all the geometry for the fusion source in the SSFR were slightly lower than the system with the ADS

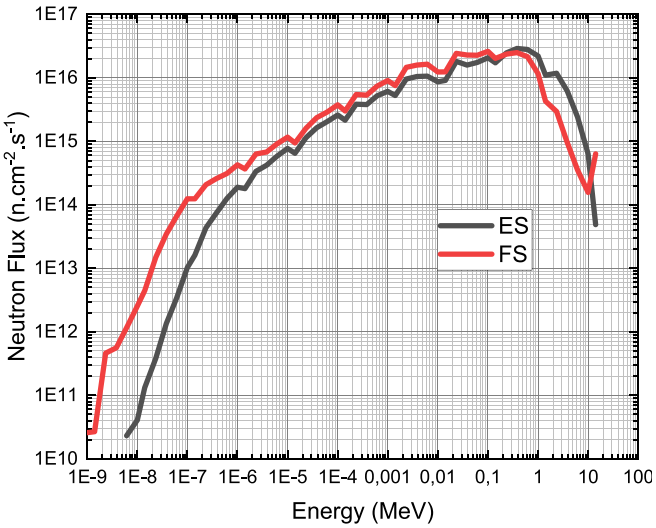

Fig. 4. Neutron flux from different external sources in SSFR.

Table 3
k_{eff} values for different sources in SSFR.

External Source	k_{eff}	Absolute difference (pcm)
ES	0.96819 ± 0.00011	25
FS	0.96794 ± 0.00011	

Table 4
Neutronic parameters at full power in SSFR for different external sources.

	ES	FS	Absolute difference
ν	2.943	2.943	0
η (all cells with fission)	1.1354	1.1367	1.3E-03
η (all system)	0.97365	0.97348	1.7E-04
f	0.93057	0.93019	3.8E-04
ε	1.5305	1.5306	1.0E-04
u	1.9738	1.9720	1.8E-03
l	5.8943E-05 s	5.9149E-05 s	2.06E-07 s
β_{eff}	3.3465E-03	3.6056E-03	2.591E-04
σ_γ/σ_f	252.39	251.94	0.45

external source. This contrast in η values is due to differences in the neutron spectrum and the capture-to-fission ratio for the system using distinct external neutron sources.

Similarly, the value of f is slightly lower when using a fusion source compared to the evaporation source in the SSFR. It indicates that thermal neutrons are more efficiently absorbed in the fuel of the SSFR using the evaporation source than the fusion source. Once again, the differences in neutron flux over the core due to the influence of the external neutron source spectrum could explain the differences in f values between both systems.

The ε values are almost the same, with an absolute difference of 10^{-4} due to the same fuel composition in both analyses, which presented that the type of external source did not directly influence the ε parameter.

On the one hand, the SSFR with the FFS external source exhibited the lowest lethargy, maintaining a hardened neutron spectrum. On the other hand, even though the values of l in seconds (s) were very low, the SSFR with the evaporation source presented slightly lower values than the fusion source in the system.

Concerning the β_{eff}, there was a higher value for the FS than the ES in the system. The high β_{eff} increases the reactor period, enhancing reactor control and safety rather than prompt fission neutrons. Despite this, the great β_{eff} could increase the probability of neutron absorption in the resonance energy range at fuel, which could explain the slightly higher k_{eff} values for the ES than the FS.

Regarding the SSFR with an external neutron source, although the difference in σ_γ/σ_f was relatively small, the system with a fusion external source presented lower σ_γ/σ_f values than the evaporation external source, indicating a higher rate of fission reactions in the system using D-T fusion source than the spallation source. The high σ_γ/σ_f values were due mainly to the breeder core, which Th radioactive capture is quite significant. Since the fuel and coolant compositions are the same in both analyses, the neutron flux over the core and the external neutron source spectrum could explain these differences in the neutronic parameters in the SSFR, even if they are very small.

Fig. 5 illustrates the neutron spectra of the SSFR's inner, outer, and breeder cores. In the inner core, the thermal neutron flux is higher for the system using the fusion source than the SSFR using the evaporation source, indicating a higher probability of inducing fission reactions in fissile materials. These differences in neutron flux directly influence the distinctions in the k_{eff} values, especially in the thermal utilization factor (f) and the average fission neutrons produced per neutron absorbed (η) for the system using different external neutron sources, as previously presented in this work. For the outer core, the neutron flux is almost the same for evaporation and fusion external sources in the SSFR, except for the thermal neutron range, in which the FS presented a higher neutron flux than the ES. Considering the system at BOL, the flux is lower than the inner and outer cores due to this reactor layer's lack of fissile nuclides.

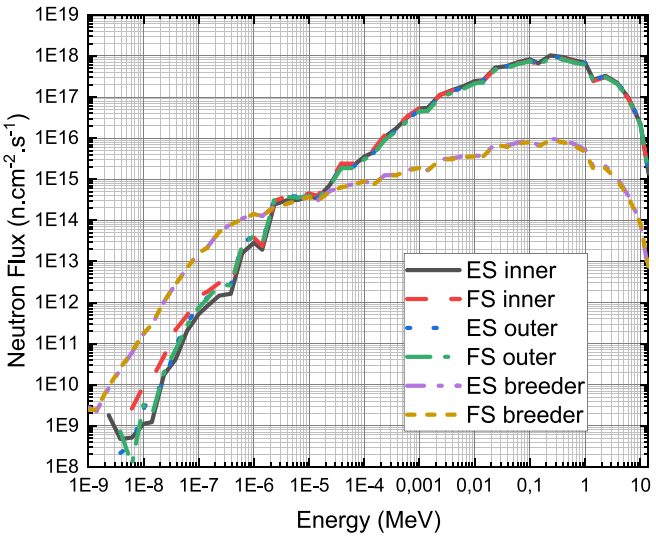

Fig. 5. Neutron flux for external sources in SSFR over inner, outer, and breeder core.

3.2. Fuel burnup simulation

Table 5 shows the neutronic parameters for the BOL and the EOL for the different external neutron sources in the SSFR. The values of ν decreased after the fuel burnup but remained the same for the external sources analyzed in the SSFR. There was a more significant reduction in the η value for the FS than the ES, which could indicate a higher neutron economy in the system with the ES than the FS.

The f values for the evaporation source increased more than the fusion source at the EOL, which increased the probability of neutron absorption in the fuel. In addition, although the reduction in the ε value was smaller for the FS than the ES, it remained slightly higher for the evaporation source than the fusion source at the EOL. The SSFR with the fusion external source remained with the lowest lethargy, maintaining a hardened neutron spectrum. Although the values of l (in seconds) were relatively low, the SSFR with the evaporation source presented very slightly lower values than the one for the fusion source in the system, which could indicate high neutron absorption in fuel material.

On the one hand, there was a higher reduction in the β_{eff} values using the fusion source than the evaporation source at the EOL. On the other hand, the σ_γ/σ_f values have decreased considerably due to the neutron absorption by Th-232 producing U-233, mainly in the breeder core, which increases the fission probability in the system. Furthermore, the evaporation source had a slightly lower σ_γ/σ_f value at the EOL than the fusion source, which also could increase fission reactions in the SSFR with the evaporation external source.

Fig. 6 presents the k_{eff} values during fuel burnup in SSFR with different external neutron sources. Although they exhibit similar behaviors, the SSFR with the evaporation external source shows higher k_{eff} values than the fusion external source over time. Furthermore, the choice of external source in SSFR highlights the importance of neutron balance during a fuel burnup simulation.

Fig. 7 shows the infinite multiplication factor (k_∞) for the external sources during the fuel burnup in SSFR. The k_∞ values increased over time due to the fission reactions in fuel over the system – and not considering neutron leakage.

Fig. 8 presents the neutron flux distribution over the core for three different instants of the fuel burnup simulation. There was a little

Table 5
Neutronic parameters differences at the EOL of the fuel in SSFR.

	ES		FS		Absolute difference between BOL and EOL	
	BOL	EOL	BOL	EOL	ADS	FFS
ν	2.943	2.866	2.943	2.866	0	0
η (all cells with fission)	1.1354	1.1174	1.1367	1.1163	−1.8E-02	−2.04E-02
η (all system)	0.97365	0.95893	0.97348	0.95768	−1.472E-02	−1.580E-02
f	0.93057	0.93582	0.93019	0.93525	5.25E-03	5.06E-03
ε	1.5305	1.5240	1.5306	1.5245	−6.5E-03	−6.1E-03
u	1.9738	2.0349	1.9720	2.0328	6.11E-02	6.08E-02
l	5.8943E-05 s	5.9161E-05 s	5.9149E-05 s	5.9628E-05 s	2.18E-07 s	4.79E-07 s
β_{eff}	3.3465E-03	3.0224E-03	3.6056E-03	3.1216E-03	−3.241E-04	−4.840E-04
σ_γ/σ_f	252.39	13.245	251.94	13.334	−238,60	−239,15

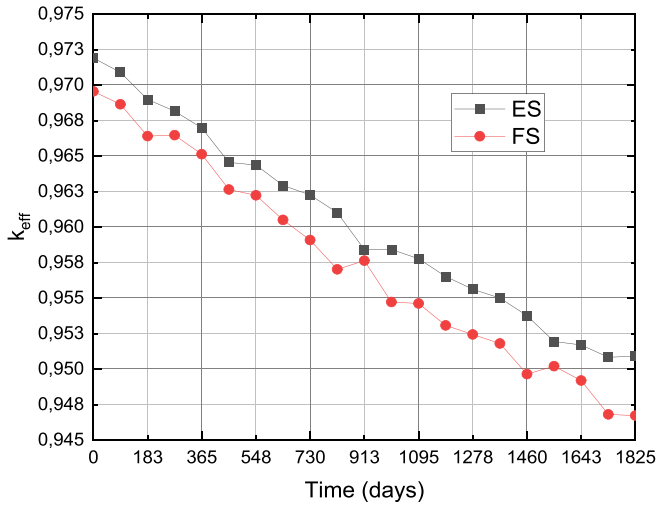

Fig. 6. k_{eff} values during fuel burnup in SSFR.

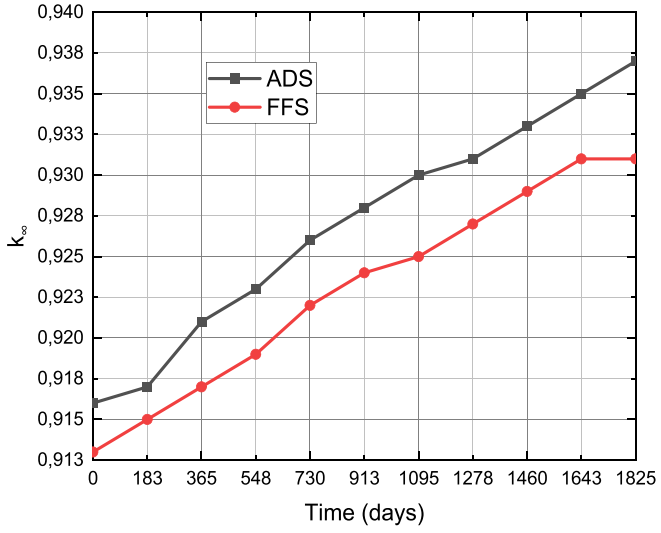

Fig. 7. Infinite multiplication factor values during fuel burnup in SSFR.

reduction in the neutron flux during the fuel burnup for both evaporation and fusion external sources, which shows the importance of the external source in the system. Furthermore, there was a more significant reduction in the neutron flux in the breeder core than in the inner and outer cores due to the highest capture-to-fission ratio in the breeder region. The neutron flux over the inner core is higher for the fusion source than the evaporation source in the thermal energy range, as shown in Fig. 8-a. It could increase the probability of inducing fission reactions in fissile materials using the fusion source in SSFR. The neutron flux over the outer core is practically the same for evaporation and fusion sources, as presented in Fig. 8-b. Moreover, the neutron flux over the breeder core is much higher in the epithermal and thermal energy ranges than the inner and outer cores, which could enhance the production of U-233 by neutron absorption in Th-232 and the probability of fission reactions in U-233 in the breeder core, as shown in Fig. 8-c.

Fig. 9 shows the capture-to-fission ratio during fuel burnup for different core regions. The fusion source presented a higher σ_γ/σ_f ratio in the inner core than the evaporation source over time, as presented in Fig. 9a. About the outer core, the values were very similar; the fusion source had slightly lower values in some time steps, as shown in Fig. 9b. The σ_γ/σ_f ratio in the breeder core is significantly higher than in the inner and outer cores due to the high Th-232 amount in the breeder core. Additionally, the ratio decays exponentially, which increases the fission probability primarily because of the increasing amount of U-233 during the fuel burnup (demonstrated later in this work), as shown in Fig. 9c. While the capture-to-fission ratio increases in the outer core, it decreases in the inner core, mainly for the ADS, which may indicate the lower k_{eff} values in the system with the fusion external source than the evaporation external source.

Fig. 10 shows the power density in the SSFR during fuel burnup, representing the sum of power densities in the inner, outer, and breeder cores for each external source. The fusion source in SSFR had the highest power density values during fuel burnup, releasing more energy over time in SSFR using the fusion external source than SSFR using the evaporation external source.

Fig. 11 and Fig. 12 show the burnup in gigawatts-day per ton of heavy metal in SSFR for the ES and the FS, respectively, during the fuel burnup simulation. The burnup over time had practically the same values and behavior during the fuel burnup, considering the fusion and the evaporation of external sources. The burnup values over time are significantly lower in the breeder core than in the inner and outer cores. Nevertheless, the inner core burnup values are twice the outer core values.

Fig. 13 presents the activity (in Curie) during the fuel burnup for each external neutron source in SSFR. The activity values remained similar over time for the fusion and evaporation sources. The activity had a high decrease in the first year of fuel burnup. It remained almost constant for the rest of the burnup because the nuclides reached the secular equilibrium after this time. It indicates that burnup time can be shortened for transuranic transmutation purposes in the SSFR.

Table 6 shows the total mass variation of minor and major actinides for the analyzed isotopes after the fuel burnup simulation for each external neutron source in the SSFR. The positive values represent a buildup, and the negative values represent a depletion of the isotopes after the fuel burnup simulation.

Concerning the uranium isotopes, there was a significant buildup of U-233 due to radioactive capture in Th-232, with values similar for both the evaporation and fusion external sources in SSFR. The U-233 production exceeded 200 kg for each case, which could be used for energy

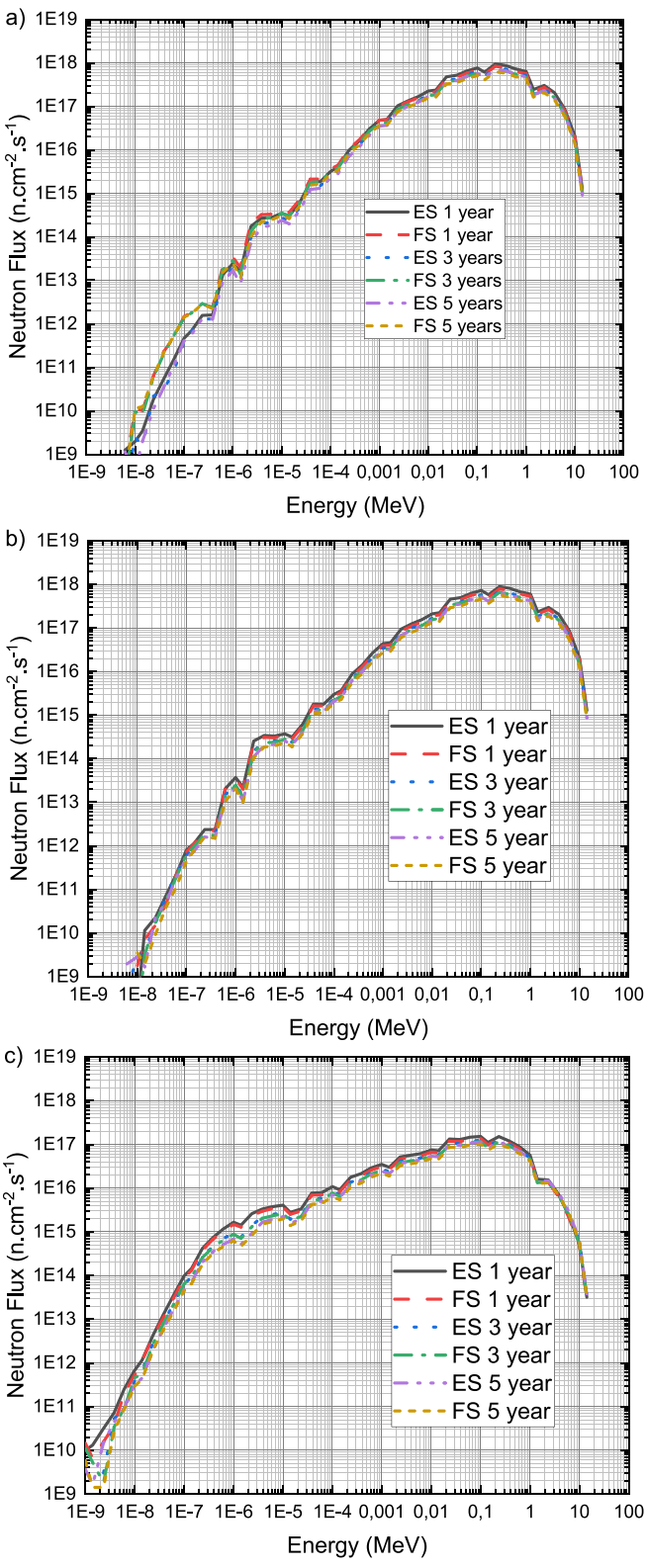

Fig. 8. Neutron flux in SSFR during the fuel burnup simulation over: a) the inner core; b) the outer core; c) the breeder core.

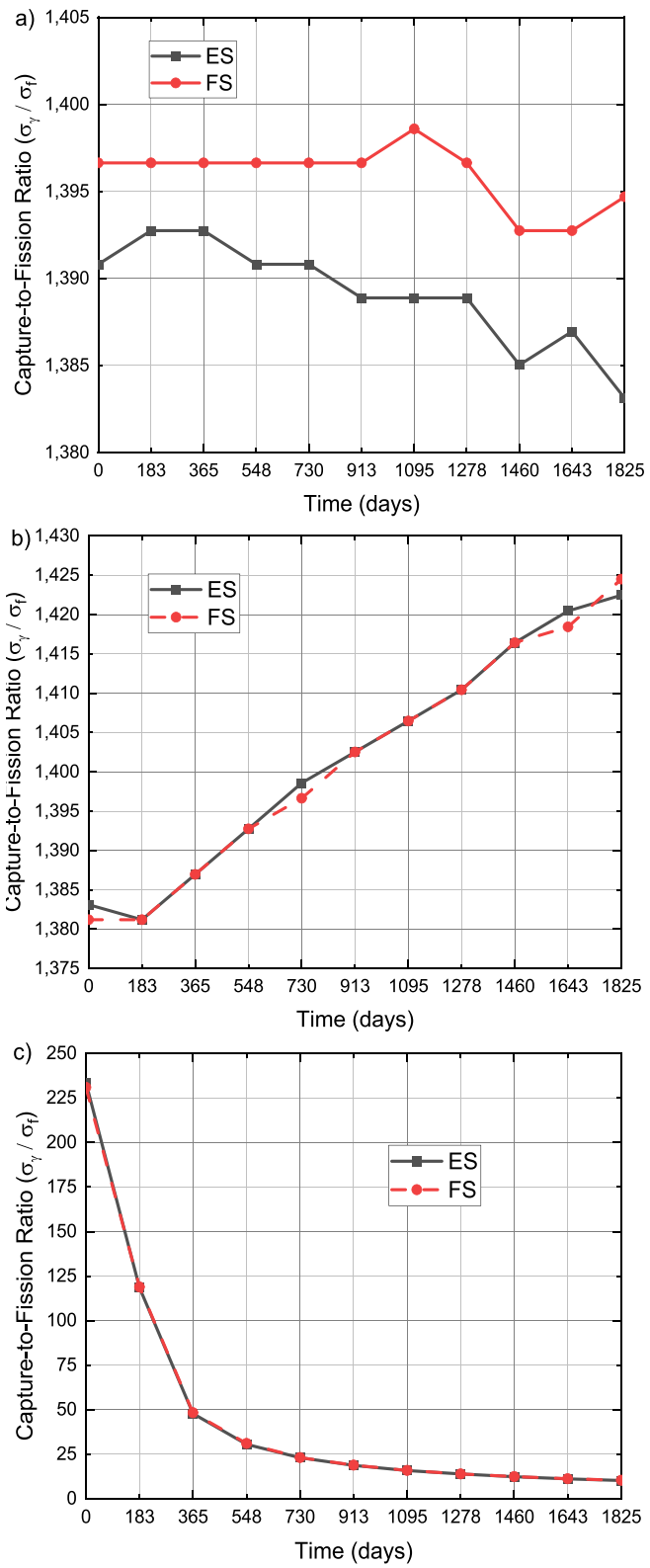

Fig. 9. Capture-to-Fission Ratio in SSFR during fuel burnup over: a) inner core; b) outer core; c) breeder core.

generation in conventional reactors such as Light Water Reactors (LWR). On the one hand, the U-232 presented the highest buildup; the values were slightly higher for the fusion source than the evaporation source. On the other hand, the U-238 showed the most significant depletion between them, where the values were almost the same for the analyzed cases. Despite the total uranium buildup being very similar between the fusion and the evaporation of external neutron sources, the ES presents a slightly more significant uranium buildup amount than the FS, which could indicate less uranium transmutation by fission reactions in SSFR with the fusion as an external neutron source.

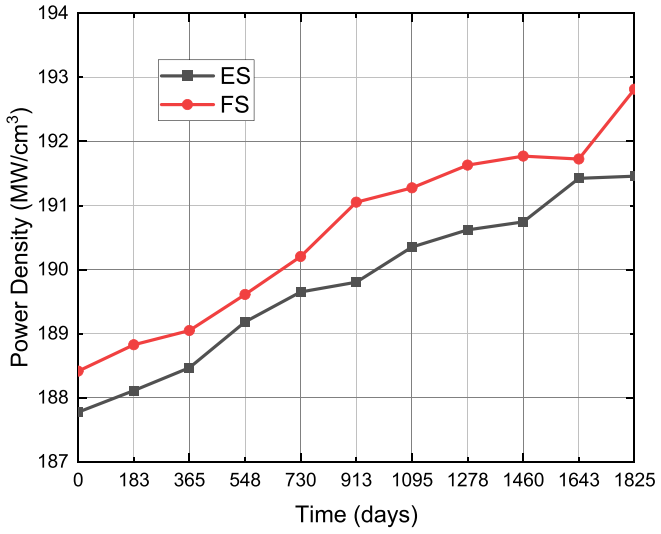

Fig. 10. Power Density in SSFR during fuel burnup.

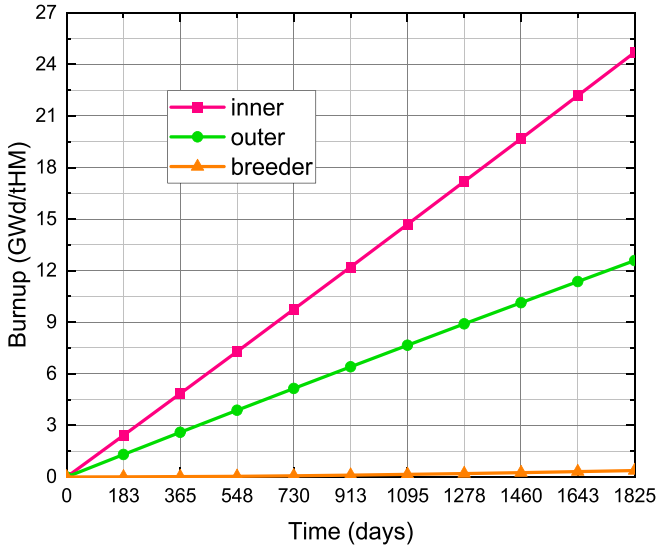

Fig. 11. Burnup in GWd/tHM in SSFR for the evaporation source.

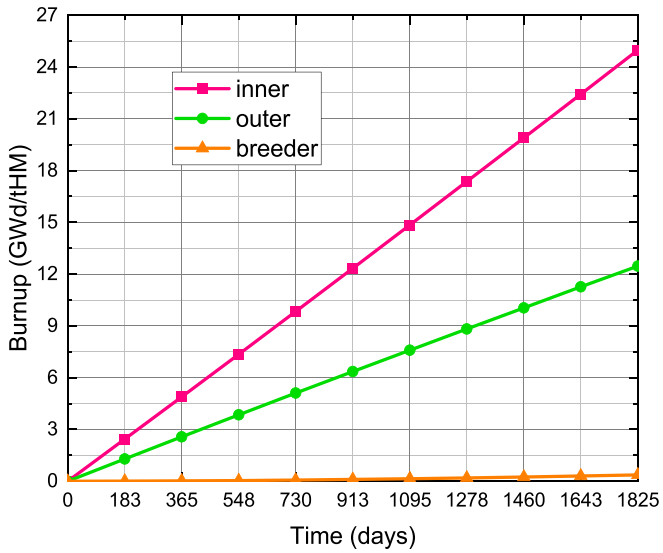

Fig. 12. Burnup in GWd/tHM in SSFR for the fusion source.

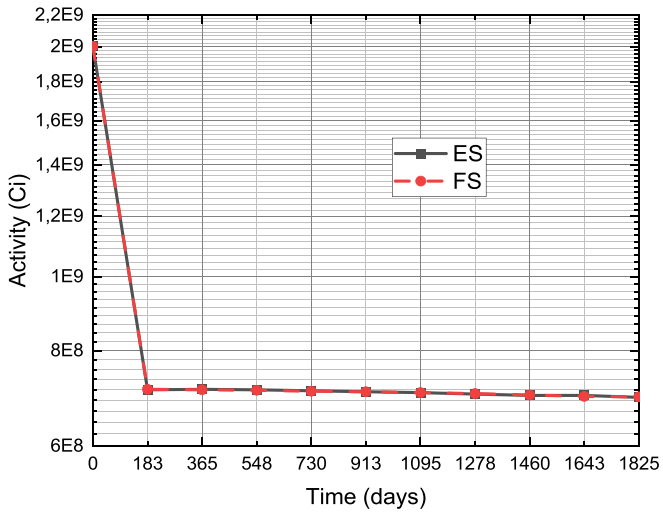

Fig. 13. Activity for different external sources in SSFR.

Regarding the plutonium isotopes, the total plutonium depletion, considering that the entire core was similar for the fusion and the external evaporation sources. In addition, Pu-239 and Pu-241 had a more significant influence on the total Pu depletion than the other Pu isotopes, respectively. About the external neutron source, the mass variation of the Pu isotopes was quite similar for the evaporation and the fusion of external neutron sources after the fuel burnup simulation.

To the mass variation of the minor actinides in SSFR after the fuel burnup simulation, the main difference between them is for Am, which could indicate that some depleted plutonium (Pu) becomes Am, especially Am-241, through radioactive capture rather than fission reactions, as already shown in this work. Moreover, the most significant minor actinide mass variation was for Am, in which Am-241 had much higher values than Am-242 ^{m} and Am-243 buildups. The Am-241 had almost 60 kg of buildup after the fuel burnup simulation, representing part of Pu decays in Am. Similar values of Am-241 buildup concerning the fusion source and the evaporation source in SSFR presented that the external source choice had a low influence on Am buildup.

In addition, all the Np isotopes had depletion in their amounts, mainly for Np-237, in which the fusion source had a slight depletion than the evaporation source. The Np-238 had such an influence on Np depletion. The Np-239 depletion was relatively low for both analyses. Furthermore, the Cm isotopes had the lowest mass variation in SSFR above all minor actinides. Concerning the external source, there were no differences between them. In both analyses, only the Cm-242 had a depletion but also presented the highest mass variation between Cm isotopes. The second one with the most impact in Cm amount was the Cm-244, which had more than 1 kg of buildup.

Concerning the radiotoxicity levels, Fig. 14 shows the ingestion radiotoxicity for the distinct external sources in SSFR. The levels of radiotoxicity by ingestion (solid elements) remained similar for the fusion and the evaporation of external neutron sources during the fuel burnup simulation, which could indicate a similar amount of actinides for both external sources in SSFR. As shown later, the ingestion radiotoxicity levels decrease until half of the fuel burnup and then increase due to americium production.

The inhalation radiotoxicity levels for the external sources in SSFR are shown in Fig. 15. The levels of radiotoxicity by inhalation (gaseous elements) for the fusion source were more significant than the evaporation source over time, which could indicate more fission products being formed in SSFR with the fusion external source.

The fission product buildup in the SSFR for each external neutron

Table 6
Total mass variation of minor and major actinides after the fuel burnup simulation in the SSFR.

Isotope	Δm (kg)	
	ES	FS
U-232	7.122E-02	7.319E-02
U-233	2.033E + 02	2.021E + 02
U-234	4.735E + 00	4.768E + 00
U-235	−6.037E-02	−5.788E-02
U-236	2.150E-01	2.146E-01
U-237	−7.190E-04	−7.120E-04
U-238	−4.94E + 00	−5.00E + 00
Np-237	−1.182E + 01	−1.193E + 01
Np-238	−1.145E-01	−1.145E-01
Np-239	−8.240E + 00	−8.240E + 00
Pu-238	1.077E + 01	1.091E + 01
Pu-239	−1.312E + 02	−1.316E + 02
Pu-240	1.142E + 01	1.191E + 01
Pu-241	−1.092E + 02	−1.094E + 02
Pu-242	3.290E + 00	3.370E + 00
Am-241	5.850E + 01	5.840E + 01
Am-242 ^{m}	1.073E + 00	1.082E + 00
Am-243	5.040E-01	5.220E-01
Cm-242	−3.800E + 00	−3.790E + 00
Cm-243	4.540E-02	5.190E-02
Cm-244	1.336E + 00	1.374E + 00
Cm-245	2.120E-01	2.200E-01
Cm-246	8.790E-03	9.050E-03

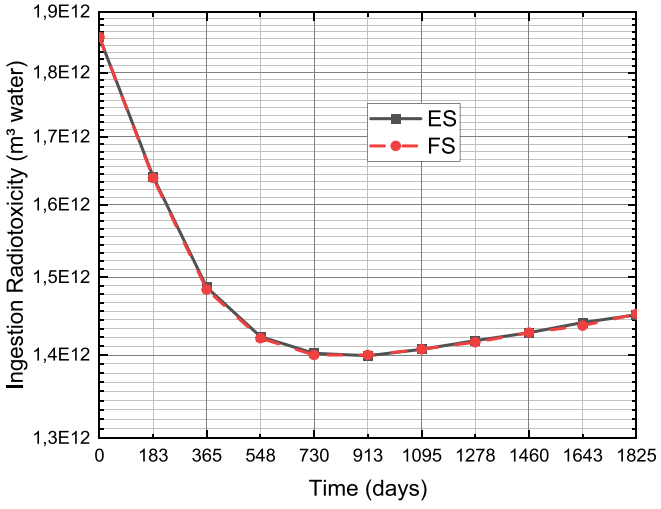

Fig. 14. Ingestion radiotoxicity for different external sources in SSFR.

source after the fuel burnup simulation is shown in Table 7. The considered fission products in the fuel burnup simulation were Kr, Sr, Y, Zr, Mo, Tc, Ru, Rh, Pd, Te, I, Xe, Cs, Ba, La, Ce, Pr, Pm, Nd, Sm, Eu, and Gd. On the one hand, the fusion source had a higher buildup in the fission production amount in the breeder and mainly in the inner core than the evaporation source due to the hardened neutron spectrum of the fusion external source in the SSFR. On the other hand, the fusion source presented lower fission production buildup in the outer core than the evaporation source. Overall, the fusion external source showed the highest fission product buildup enhancing fission reactions in actinides in the SSF. However, it increases the neutron absorption by the fission products, which could be proven by the slightly higher k_{eff} values for the evaporation source than the fusion source in the system.

Table 8 shows the transuranic transmutation through mass variation by fission reactions in the analyzed systems after the fuel burnup simulations. The breeder core was not included in transuranic mass variations because the values were negligible. The fusion source had slightly higher transmutation values in the inner core than the evaporation

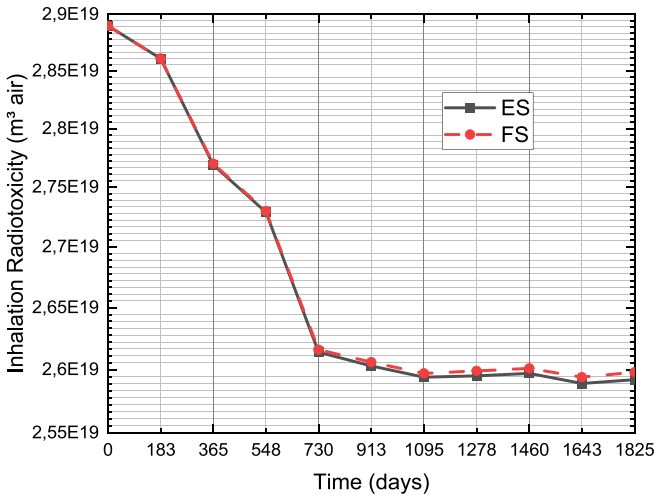

Fig. 15. Inhalation radiotoxicity for different external sources in SSFR.

Table 7
Fission products buildup after the fuel burnup in SSFR.

	Δm (kg)	
	ES	FS
inner	32.63017	33.23556
outer	38.81981	38.27320
breeder	0.5809386	0.5809448
total	72.03091	72.08970

Table 8
Transuranic mass variation after the fuel burnup in SSFR.

	Δm (kg)	
	ES	**FS**
inner	−81.59784	−82.48383
outer	−95.61777	−94.74712
total	−177.2156	−177.2309

source because of its hardened neutron spectrum. Considering the outer and the breeder cores, the evaporation source had greater transmutation values than the fusion source due to the smaller capture-to-fission ratio during the fuel burnup in the ES than in the FS.

Finally, suppose the actinides are considered, which included thorium, uranium, and protactinium (Pa) in the analysis. In that case, the transmutation by fission reactions increases after the fuel burnup simulation and changes between them, as shown in Table 9. Once more, the fusion source presented higher transmutation values than the evaporation source regarding the inner core, and the evaporation source had more transmutation than the fusion concerning the outer core. Furthermore, the SSFR with fusion external source showed slightly higher transmutation values than the evaporation source even though some neutronic parameters, such as fission-to-capture ratio and criticality, are lower for the fusion source than the evaporation source,

Table 9
Actinide mass variation after the fuel burnup in SSFR.

	Δm (kg)	
	ES	FS
inner	−97.38111	−98.25007
outer	−106.74301	−105.91878
breeder	−1.927130	−2.149080
total	−206.0512	−206.3179

especially in the breeder core. As a result, the hardened neutron flux of the fusion external neutron source at the system increases the probability of inducing fission reactions in actinides in the SSFR, mainly in the inner and breeder cores.

4. Conclusion

In this study, the fuel burnup simulation of a Small-sized Subcritical Fast Reactor (SSFR) was analyzed under distinct external neutron sources, such as evaporation and fusion neutron sources. The results indicated that both external neutron sources, fusion, and evaporation, produced satisfactory and very similar outcomes. For all practical purposes, there are no significant differences between the two approaches based on the presented data. While the fusion source appears to yield slightly better results than the evaporation source, for practical purposes, both approaches seem equally suitable according to the presented data. Overall, the hardened neutron flux of the fusion external neutron source at the system increases the probability of inducing fission reactions in actinides in the SSFR, mainly in the inner and breeder cores. At the same time, the evaporation external neutron source presents higher transmutation values in the inner core due to its hardened neutron spectrum.

Both neutron sources demonstrated effectiveness in nuclide transmutation and reducing fuel radiotoxicity. The overall results showed high depletion rates for transuranic nuclides (approximately 177 kg) and actinides (about 206 kg), highlighting the system's efficacy in high-level radioactive waste management. Ultimately, although the fusion source may exhibit a slight advantage, the overall results indicate that both approaches are equally viable in achieving the proposed objectives. Therefore, the analysis presented in this study contributes to a better understanding of the neutronic behavior and transmutation in SSFR, which can aid in designing and optimizing such systems. Future works will analyze the neutronic parameters in the system using the fusion source studying first wall materials in plasma containment, mainly vanadium alloys, to keep a hardened neutron flux of deuterium–tritium fusion neutrons, increasing the transmutation parameters of actinides.

CRediT authorship contribution statement

Renato Vinícius A. Marques: Conceptualization, Data curation, Formal analysis, Investigation, Methodology, Validation, Writing – original draft. **Carlos E. Velasquez:** Formal analysis, Investigation, Supervision, Validation, Writing – review & editing. **Claubia Pereira:** Conceptualization, Formal analysis, Funding acquisition, Investigation, Project administration, Resources, Software, Supervision, Validation, Writing – review & editing.

Declaration of competing interest

The authors declare that they have no known competing financial interests or personal relationships that could have appeared to influence the work reported in this paper.

Data availability

Data will be made available on request.

Acknowledgments

The authors are grateful to the Brazilian research funding agencies, CNEN (Brazil), CNPq (Brazil), CAPES (Brazil), and FAPEMIG (MG/Brazil) for the support.

References

Nuclear Energy Agency (NEA), Organization for Economic Co-operation and Development (OECD), Accelerator-driven Systems (ADS) and Fast Reactors (FR) in Advanced Nuclear Fuel Cycles - A Comparative Study, 2002.

Nuclear Energy Agency, JEFF-3.3 evaluated data library, 2017, https://www.oecd-nea.org/dbdata/jeff/jeff33/index.html.

Aneheim, E.H.K., 2012. Development of a Solvent Extraction Process for Group Actinide Recovery from Used Nuclear Fuel, Department of Chemical and Biological Engineering. CHALMERS UNIVERSITY OF TECHNOLOGY, Gothenburg, Sweden.

Barros, G., Carvalho, K.A., Velasquez, C.E., Santos, A., Vasconcelos, V., Campolina, D., Pereira, C., "Comparison of spallation and fusion neutron sources in fuel transmutation and regeneration", Annals of Nuclear Energy, ELSEVIER – June 2021, https://doi.org/10.1016/j.anucene.2021.108159.

Bedenko, S.V., Lutsik, I.O., Prikhodko, V.V., Matyushin, A.A., Polozkov, S.D., Shmakov, V.M., Vega-Carrillo, H.R., 2022. "Fusion-fission hybrid reactor with a plasma source of deuterium-tritium neutrons in a linear configuration", Progress in Nuclear Energy 154. ELSEVIER 104477. https://doi.org/10.1016/j.pnucene.2022.104477.

Cota, S., Pereira, C., 1997. Neutronic evaluation of the non-proliferating reprocessed nuclear fuels in pressurized water reactors. Ann. Nucl. Energy 24 (10), 829–834. https://doi.org/10.1016/S0306-4549(96)00051-5.

Croff, A., A USER'S MANUAL FOR THE ORIGEN2 COMPUTER CODE, ORNL/TM-7175, 1980.

Deng, N., Xie, J., Hou, C., Zeng, W., Chen, Z., Yu, T., Zhao, P., Liu, Z., Xie, C., Xie, Q., 2021. Dynamic Characteristics of Accelerator-Driven Subcritical Reactor With Self-Adapting Multi-Mode Core Few-Group Constants. Frontier in Energy Research 8, 603084. https://doi.org/10.3389/fenrg.2020.603084.

Esam, M.A., December 2020. Hussein, "Emerging small modular nuclear power reactors: A critical review", Physics Open, Volume 5. ELSEVIER. https://doi.org/10.1016/j.physo.2020.100038.

Gilberti, M., Pereira, C, Veloso, M.A.F., Costa, A.L., "Transuranics Transmutation Using Neutrons Spectrum from Spallation Reactions", Science and Technology of Nuclear Installations, v. 2015, p. 23, 2015, doi:10.1155/2015/104739.

De-peng Guo, Fei Xie, Jing Zhao, "Research and Comparison of Solid Spallation Targets in Accelerator Driven System (ADS)", Advances in Engineering Research, volume 94, 2nd International Conference on Sustainable Development (ICSD), 2016, doi: 10.2991/icsd-16.2017.126.

Hong, S.H., Kim, M.H., 2018. "Neutronic investigation of waste transmutation option without partitioning and transmutation in a fusion-fission hybrid system", Nuclear Engineering and Technology 50. ELSEVIER 1060–1067. https://doi.org/10.1016/j.net.2018.06.008.

International Atomic Energy Agency (IAEA), Climate Change and Nuclear Power, Securing Clean Energy for Climate Resilience, 2022.

International Atomic Energy Agency (IAEA), Thorium Fuel Cycle - Potential Benefits and Challenges, ISSN 1011–4289, 2005.

Lafuente, A., Piera, M., "Nuclear fission sustainability with subcritical reactors driven by external neutron sources", Annals of Nuclear Energy, ELSEVIER – April 2011, https://doi.org/10.1016/j.anucene.2010.11.024.

MacFarlane, R.E., "The NJOY Nuclear Data Processing System, Version 2012", Los Alamos National Laboratory, LA-UR-12-27079, 2012.

Marques, R.V.A., Saturnino, M., Martins, F., Velasquez, C.E., Pereira, C.M.A.F., Costa, A. L., 2020. Tritium Breeder Layer Evaluation of Fusion-Fission Hybrid System. Fusion Sci. Technol. 76 (2), 145–152. https://doi.org/10.1080/15361055.2019.1704594.

Miguirditchian M., L. Chareyre,, L., Sorel, C., Bisel, I., Baron, P., Masson, M., "Development of the GANEX Process for the Reprocessing of Gen IV Spent Nuclear Fuels", ATALANTE Conference 2008, Montpellier (France), 2008.

Ogata, T., Kim, Y., Yacout, Y., 2020. Metal Fuel Performance Modeling and Simulation. Comprehensive Nuclear Materials (second Edition) 5, 43–87. https://doi.org/10.1016/B978-0-08-056033-5.00075-6.

Plukienė, R., Plukis, A., Juodis, L., Remeikis, V., Šalkauskas, O., Ridikas, D., Gudowski, W., 2018. "Transmutation considerations of LWR and RBMK spent nuclear fuel by the fusion–fission hybrid system", Nuclear Engineering and Design 330. ELSEVIER 241–249. https://doi.org/10.1016/j.nucengdes.2018.01.046.

Poston, D., Trellue, H., USER'S MANUAL, Version 2.0 for Monteburns Version 1.0.LA-UR-99-4999, 1999.

Lei Ren, Zi-Wei Li,Yun-Cheng Han,Xiao-Yu Wang,Jia-Chen Zhang, "Neutronics study of a subcritical system driven by external neutron source for 99Mo production", Fusion Engineering and Design, ELSEVIER – April 2021, https://doi.org/10.1016/j.fusengdes.2021.112263.

Rubbia, C., Rubio, J.A., Buono, S., Carminati, F., Fiétier, N., Gálvez, J., Gelès, C., Kadi, Y., Klapisch, R., Mandrillon, P., Revol, J.P.C., Roche, C., 1995. Conceptual design of a fast neutron operated high power energy amplifier. CERN-Group, European Organization of Nuclear Research.

Şahin, S., Şahin, H.M., Tunç, G., 2018. "Monte Carlo analysis of LWR spent fuel transmutation in a fusion-fission hybrid reactor system", Nuclear Engineering and Technology 50. ELSEVIER 1339–1348. https://doi.org/10.1016/j.net.2018.08.006.

Saito, S., Tsujimoto, K., Kikuchi, K., Kurata, Y., Sasa, T., Umeno, M., Nishihara, K., Mizumoto, M., Ouchi, N., Takei, H., Oigawa, H., 2006. "Design optimization of ADS plant proposed by JAERI", Nuclear Instruments and Methods in Physics Research A 562. ELSEVIER 646–649. https://doi.org/10.1016/j.nima.2006.02.078.

Tran Minh, T., "Analyzing the Neutron Parameters in the Accelerator Driven Subcritical Reactor Using the Mixture of Molten Pb-Bi as Both Target and Coolant", Atoms 2021, 9, 95 (2021), https://doi.org/10.3390/atoms9040095.

Velasquez, C.E., Pereira, C., Veloso, M.A.F., Costa, A.L., Barros, G., "Fusion–Fission Hybrid Systems for Transmutation", Journal of Fusion Energy, Volume 35 – Number 1, pg 1-134, 2016, https://doi.org/10.1007/s10894-016-0080-3.

X-5 Monte Carlo Team, Mcnp, "A General Monte Carlo N-Particle Transport Code, Version 5", vol. II. User's Guide University of California, Los Alamos National Laboratory, 2003.

Zafar, Z.I., Myung Hyun Kim, M.H., "Embedded fission source approach to analyze external source effect in a subcritical reactor", Nuclear Engineering and Design, ELSEVIER – February 2018, https://doi.org/10.1016/j.nucengdes.2017.11.039.

Zhivkov, P., Chavdar Stoyanov, C., Furman, W., "Accelerator driven system for transmutation and energy production", EPJ Web of Conferences 194 (08002), 2018, https://doi.org/10.1051/epjconf/201819408002.